Supporting Information for:

Selective detection of SO_2 in NU-1000 *via* organometallic nickel silylphosphine post-synthetic complex incorporation

Juan L. Obeso,[a,b,†] Luz J. Barrios-Vargas,[c,†] Valeria B. López Cervantes,[a,†] Yoarhy A. Amador-Sánchez,[a] Nancy Martin-Guaregua,[d] Ricardo A. Peralta,[d] Ramon Munoz,[e] Ana Martínez,[f] Carolina Leyva,[b] Diego Solis-Ibarra,[a] Elí Sánchez-González,[a]* Ilich A. Ibarra[a]* and Virginia Montiel-Palma[c]*

[a] Laboratorio de Fisicoquímica y Reactividad de Superficies (LaFReS), Instituto de Investigaciones en Materiales, Universidad Nacional Autónoma de México, Circuito Exterior s/n, CU, Coyoacán, 04510, Ciudad de México, Mexico.

[b] Instituto Politécnico Nacional, CICATA U. Legaria, Laboratorio Nacional de Ciencia, Tecnología y Gestión Integrada del Agua (LNAgua), Legaria 694 Irrigación, 11500, Miguel Hidalgo, CDMX, México.

[c] Department of Chemistry, Mississippi State University, Mississippi State, Mississippi 39762, United States.

[d] Departamento de Química, División de Ciencias Básicas e Ingeniería. Universidad Autónoma Metropolitana (UAM-I), 09340, México.

[e] Mississippi School for Maths and Science, 1100 College St, Columbus, Mississippi 39701, United States.

[f] Departamento de Materiales de Baja Dimensionalidad. Instituto de Investigaciones en Materiales, Universidad Nacional Autónoma de México, Circuito Exterior s/n, CU, Coyoacán, 04510, Ciudad de México, México.

[†] These authors contributed equally to this work.

Contents

S1. General Experimental Details

Analytical instrumentation

Inductively coupled plasma-mass spectrometer (ICP-MS)

The Ni and Zr metal contents in the [NiSi]@NU-1000 material were determined by ICP-MS using calibration curves prepared under the same conditions as those of the material. Then, a sample of [NiSi]@NU-1000 material was digested in a mixture of concentrated acids, dissolved and diluted. The technique gave the values of the weight percent content of each of the metals as Ni: 0.560 wt.% and Zr: 5.41 wt%. This corresponds to $9.50x10^{-5}$ mol of Ni and $5.93x10^{-4}$ mol of Zr per 100 g of sample, or 0.960 mol Ni per 6.00 mol of Zr.

X-ray absorption fine structure (XAFS)

XAFS spectra were measured at the Ni K edge on the [NiSi]@NU-1000 at the Materials Research Collaborative Access Team (MR-CAT) beamline 10-ID at Argonne National Laboratory's Advanced Photon Source. Samples were prepared in an air-free glovebox as self-supported pressed pellets and measured in transmission mode in a triple-sealed sample holder to minimize air leakage. High-purity Zr was used to prepare the NU-1000.

Powder X-Ray Diffraction Patterns (PXRD)

PXRD was collected on a PROTO Diffractometer, AXRD Benchtop with a Cu-Kα1 radiation ($\lambda = 1.5406$ Å) using a nickel filter. Patterns were recorded in the 2-50° 2θ range with a step scan of 0.02° and 2 seconds per step.

N2 isotherms

N_2 isotherms (up to $P/P_0 = 1$ and 77 K) were recorded on a micromeritics TriStar II PLUS analyzer under high vacuum in a clean system with a diaphragm pumping system. Activation was carried out at 453 K under high vacuum using a membrane pump for 16 h.

Scanning electron micrographs (SEM)

Scanning electron micrographs (SEM) images were taken using a JEOL 6500F Field Emission SEM at the Institute for Imaging and Analytical Technologies (I2AT Mississippi State University).

Energy dispersive X-ray spectroscopy (EDX)

Energy dispersive X-ray spectroscopy was performed on a Philips XL30 field emission scanning electron microscope.

Thermal gravimetric analysis (TGA)

TGA was performed using a TA Instruments Q500HR analyzer under an N_2 atmosphere using the high-resolution mode (dynamic rate TGA) at a scan rate of 5 °C min^{-1}, from room temperature to 700 °C.

Solid-state ultraviolet-visible spectroscopy (UV-Vis)

Absorption measurements were performed from 200-800 nm using a Shimadzu spectrophotometer UV-2600 equipped with an ISR-2600Plus integrating sphere and a $BaSO_4$ blank.

SO_2 adsorption experiments

For SO_2 adsorption experiments, the adsorption-desorption isotherm was recorded at 298 K and up to 1 bar using a Dynamic Gravimetric Gas/Vapor Sorption Analyzer, DVS Vacuum (Surface Measurements Systems Ltd.)

Fluorescence experiments

Emission spectra were taken in an Edinburgh Instrument FS5 fluorimeter using a continuous wave 150 W ozone-free xenon arc lamp at room temperature. They were later packed into the quartz sample holders and positioned in the instrument. Measurements were carried out using an excitation wavelength of 350 nm, with a 395 nm long-pass filter on the detector side to remove any remaining light from the excitation source. The measurements were collected with a step size of 1 nm and a dwell time of 0.2 s. The excitation bandwidth was set at 0.50 nm, and the emission bandwidth for the detector was 1.00 nm. Half-life spectra were carried out by exciting the sample with a picosecond pulsed light emitting diode EPLED-340 with an excitation wavelength of 335.6 nm, a pulse width of 930.8 ns and a bandwidth of 12.4 nm, at an emission wavelength of 500 nm.

S2. Results and Discussion

S2.1. Synthesis and characterization of [NiSi]@NU-1000

The Metal Organic Framework NU-1000 was synthesised as previously reported by Farha *et al.*[S1] In parallel, the organometallic complex [HNi(κ^4(*Si,P,P,P*)-Si(*o*-$C_6H_4CH_2PPh_2)_3$], herein [NiSi] was also synthesised by our previously reported methodology.[S2] For the grafting of the organometallic [NiSi] onto the MOF material, microcrystalline NU-1000 (56.1 mg, 0.03 mmol) was added to a 5 mL toluene solution of [NiSi] (60.6 mg, 0.07 mmol) at room temperature. After stirring for 48 h, the resultant yellow solid was centrifuged out of the suspension and washed with toluene and pentane 5 times. The solid was soaked overnight in 3 mL toluene and then dried under a dynamic vacuum for 12 h.

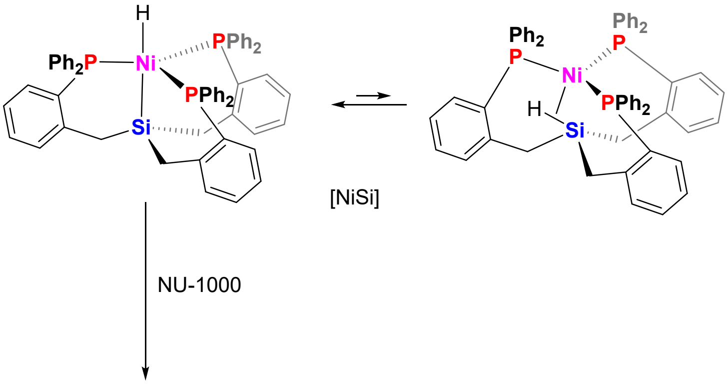

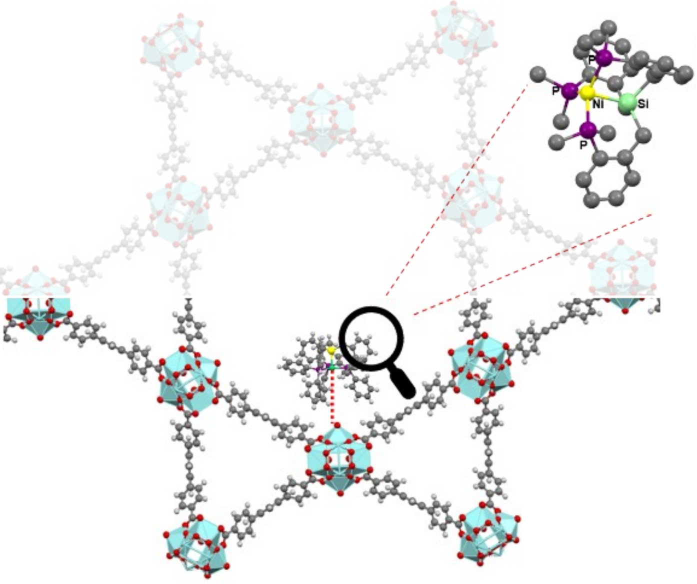

Scheme S1. The synthesis and proposed structure of the organometallic c lex grafted onto the Zr-nodes of NU-1000 giving rise to [NiSi]@NU-1000 material.

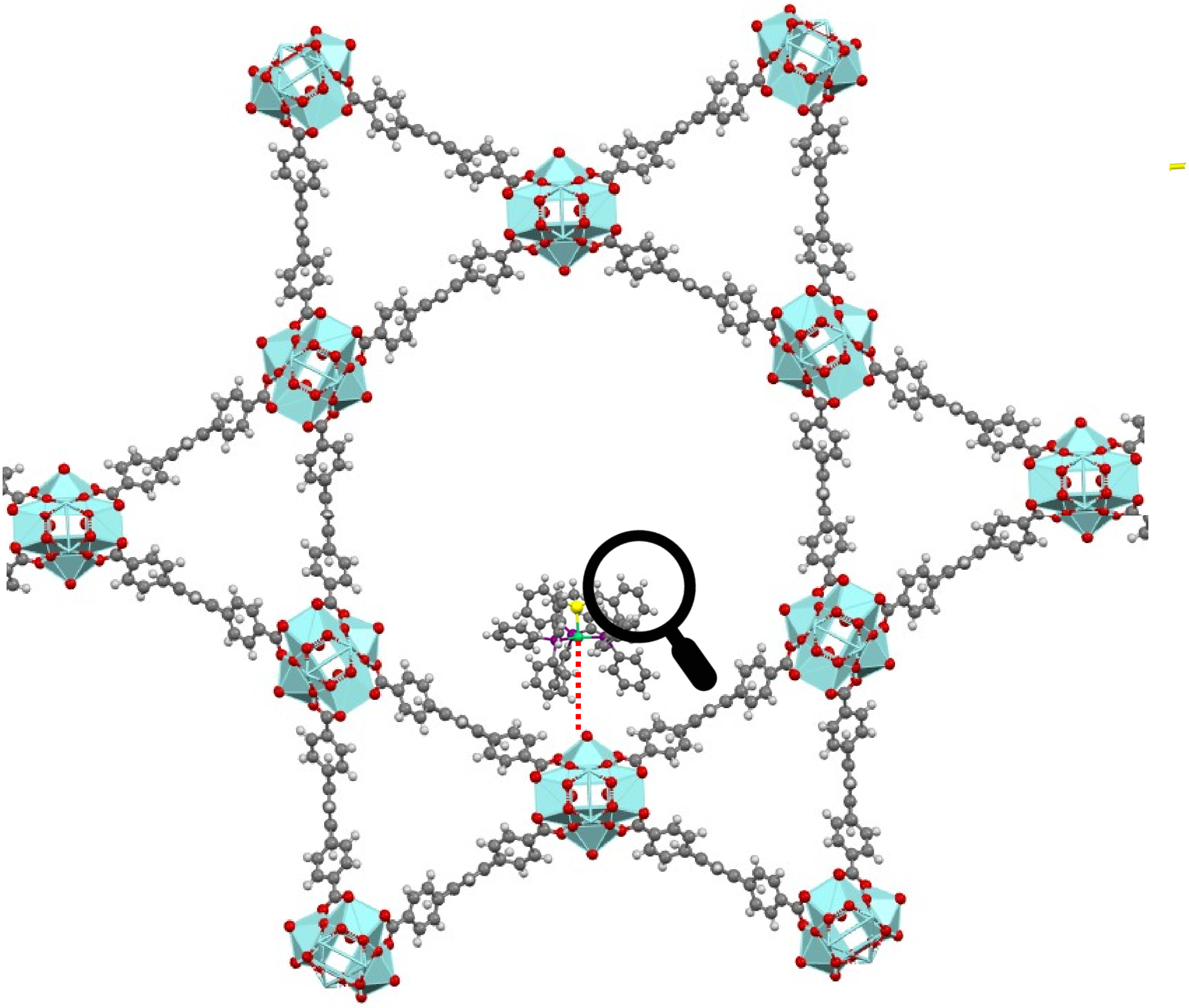

Both the organometallic [NiSi] and the [NiSi]@NU-1000 material were thoroughly characterized by a range of techniques. Organometallic [NiSi] was previously fully characterized computationally and experimentally, ^{1}H, ^{13}C, ^{29}Si, ^{31}P NMR as well as elemental analysis, IR, and single crystal X ray diffraction.[S2] Selected relevant spectra are reproduced below:

Selected NMR spectra of organometallic [**NiSi**]

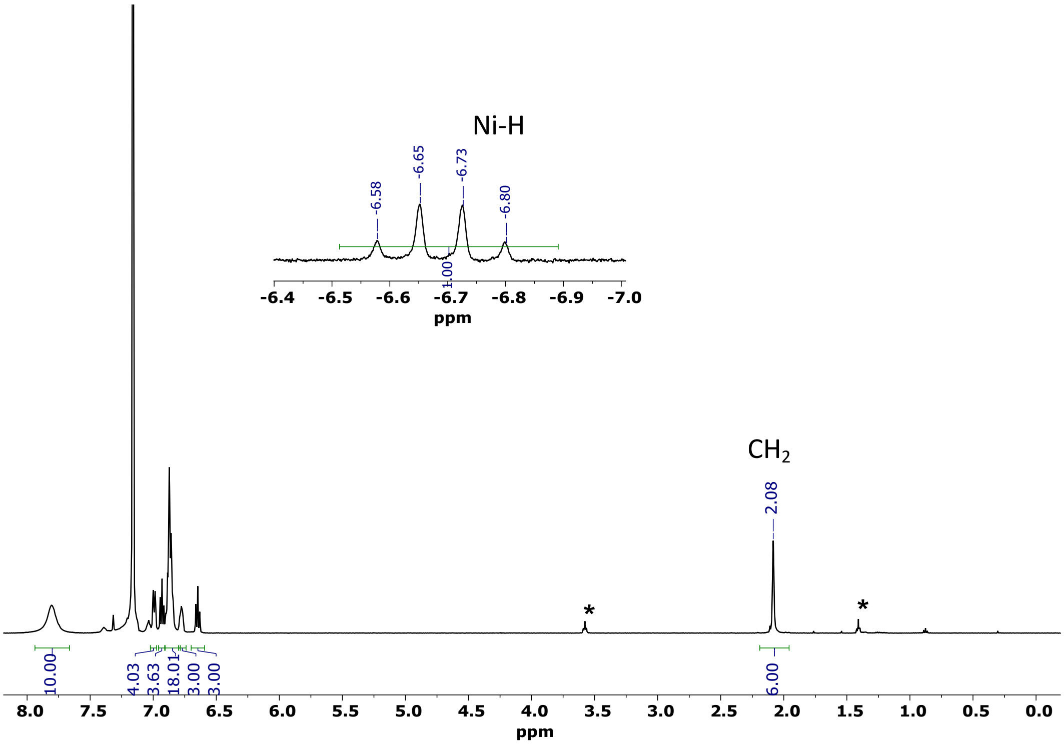

Figure S1. ^{1}H NMR spectrum (500 MHz, C_6D_6, 298 K) of precursor [NiSi].[S2](*= THF)

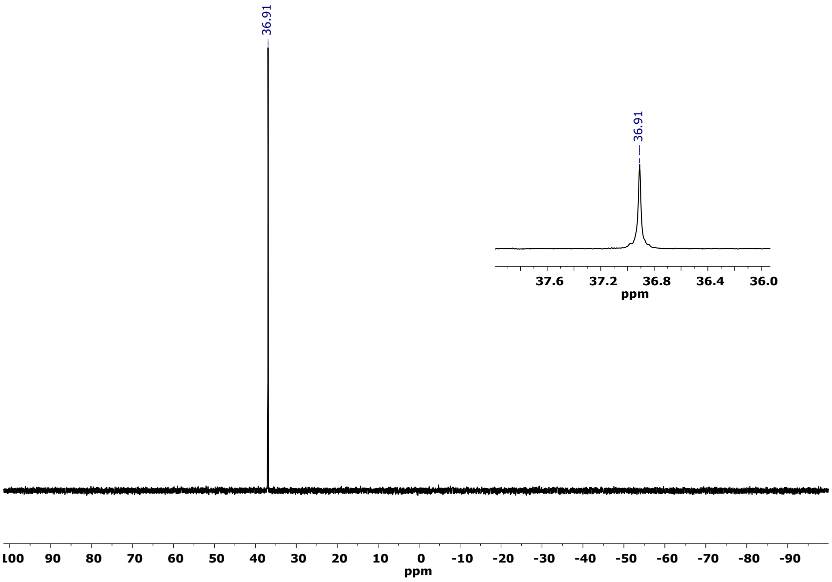

Figure S2. ^{31}P{^{1}H} NMR spectrum (202.46 MHz, C_6D_6, 298 K) of organometallic precursor [NiSi].[S2].

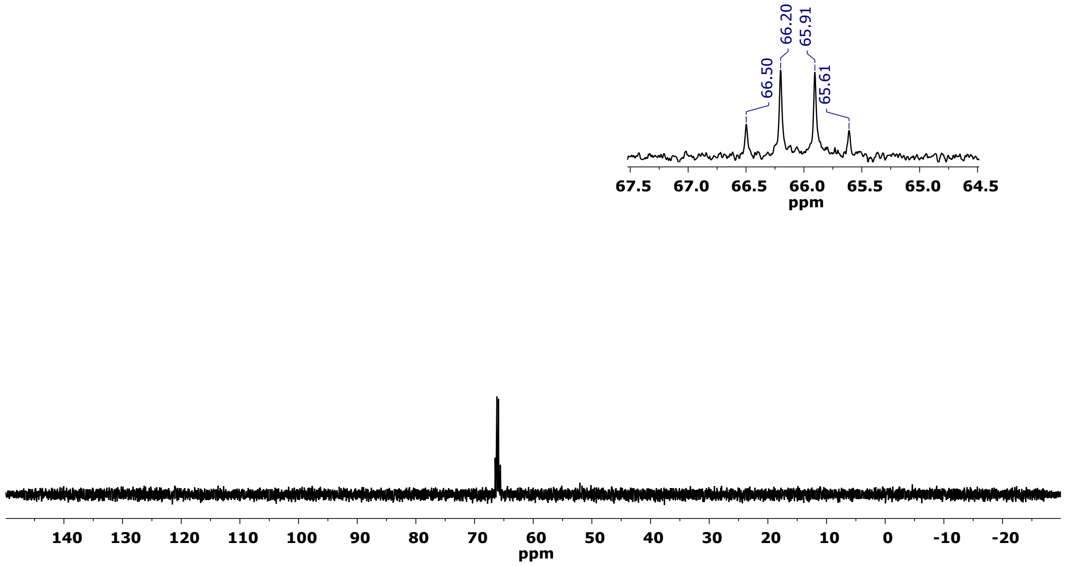

Figure S3. $^{29}Si\{^1H\}$ DEPT NMR spectrum (99.36 MHz, C_6D_6, 298 K) of organometallic precursor [NiSi].[S2]

ORTEP drawing of complex [NiSi]

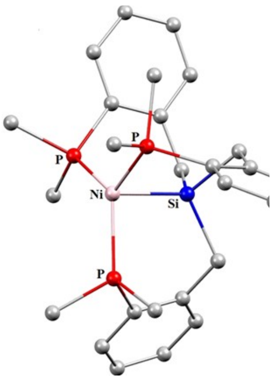

Figure S4. The solid-state structure by single crystal X-ray diffraction of organometallic precursor **[NiSi]** as in reference S2. Main bond distances (Å) and angles (°): Ni-Si 2.246(2), Ni-P1 2.1796(13), P1-Ni-P1#2 119.985(2), P1-Ni-Si1 90.74(4).[S2]

S2.2 Characterization of [NiSi]@NU-1000

The grafted material [NiSi]@NU-1000 was characterized by PXRD and BET to probe the retention of crystallinity of the NU-1000 support; ICP-MS for the determination of Ni and Zr content (as weight percent and Ni:Zr molar ratio); synchrotron XANES and EXAFS for the determination of oxidation state and coordination around Ni; SEM and EDX to confirm the homogenous distribution and presence of Zr, Ni, P and Si; as well as TGA and UV-Vis in solid state. Also, FTIR spectroscopy of the material before and after grafting of the NU-1000 with the Ni complex, and after adsorption of SO_2; and solution ^1H NMR after digestion with D_2SO_4 confirmed the presence of the original MOF fragments.

S2.2.1 PXRD analyses

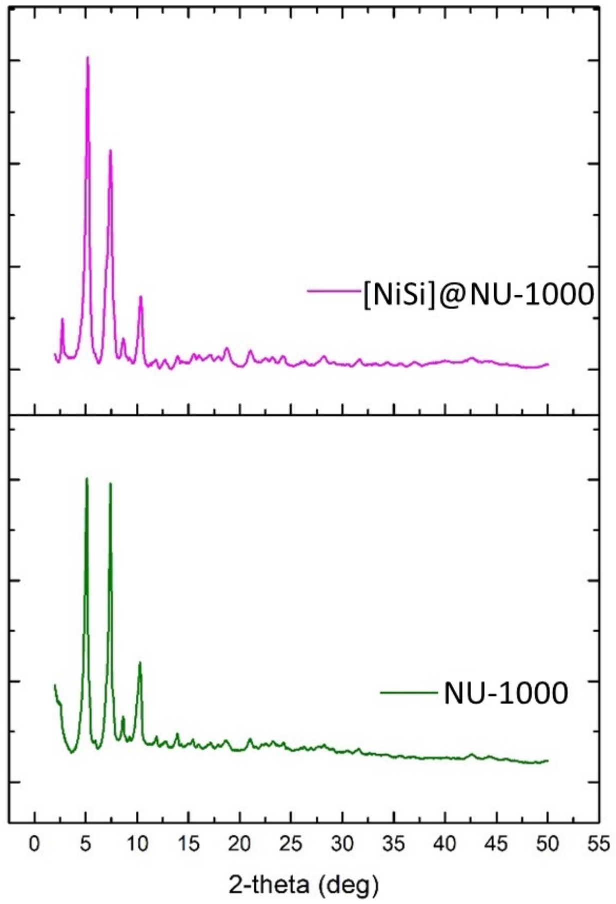

Figure S5. PXRD patterns of NU-1000 and [NiSi]@NU-1000.

The PXRD analyses confirm the retention of the crystallinity of the NU-1000 support after the incorporation of the Ni organometallic complex.

S2.2.2 N_2 adsorption-desorption isotherms

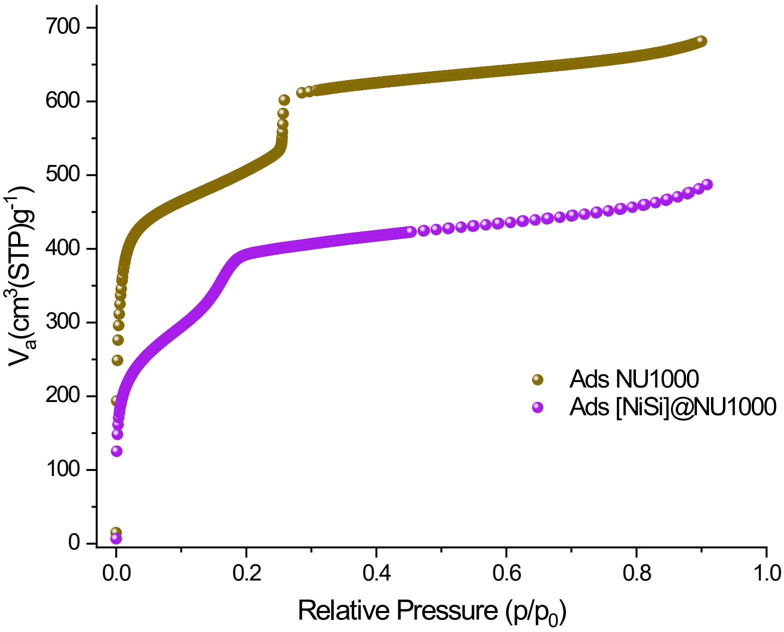

Figure S6. Nitrogen adsorption-desorption isotherms for NU-1000 and [NiSi]@NU-1000 showing a decrease in BET surface area for [NiSi]@NU-1000 (1354 m^2 g^{-1}) in comparison to as-synthesized NU-1000 (1970 m^2 g^{-1}). [S1]

Determination of BET surface area of the grafted material is in agreement with the grafting of the Ni complexes onto the pores of the material.

S2.2.3 Determination of Ni and Zr content by ICP-MS

The Ni and Zr metal contents in the [NiSi]@NU-1000 material were measured in an inductively coupled plasma-mass spectrometer (ICP-MS). The ICP-MS calibration curves were obtained with a series of standardized nickel and zirconium solutions, where nickel(II) nitrate and zirconium tetrachloride (CRM standards from Sigma Aldrich) were treated with a mixture of concentrated HNO_3 (5 mL), HCl (5 mL), H_2SO_4 (2 mL) and distilled water (13 mL). The desired standardized solutions were prepared by diluting an aliquot of the stock solution to a final volume of 10 mL of the same matrix. To perform the metal content determination of Ni-1@NU-1000, a sample was dissolved in a mixture of conc. HNO_3 (5 mL), HCl (5 mL), H_2SO_4 (2 mL), and distilled water (13 mL), then an aliquot (1.5 mL) of this solution was diluted to 10 mL with the acid matrix. The technique gave the values of weight percent content of each of the metals as given below.

Conversion of weight percent to mol gave a Ni:Zr, 0.96:6 molar ratio, very close to one Ni atom per each Zr_6 unit.

Table S1. The determination of Ni and Zr contents in material [NiSi]@NU-1000.

	Ni	Zr
Found w%	0.560	5.41
n/100 g sample	0.0000950 mol	0.000593 mol
Molar ratio	0.960	6.00
Approximate molar ratio	1	6

S2.2.4 XANES analysis of [NiSi]@NU-1000[S2]

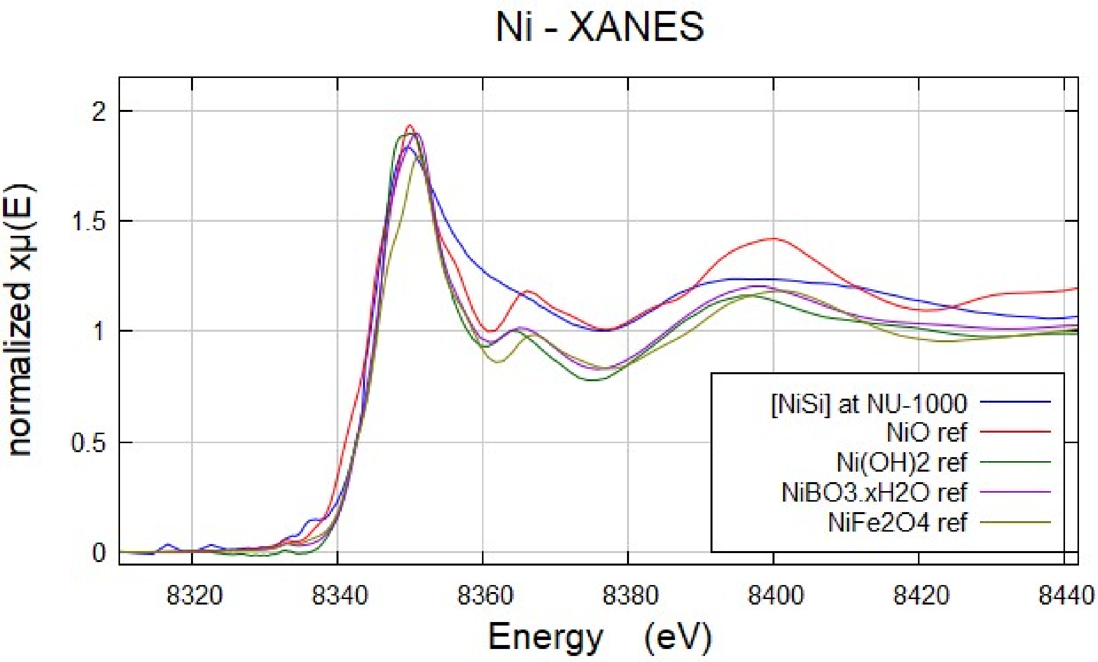

Figure S7. Transmission XANES of Ni K edge of a sample of [NiSi]@NU-1000 (blue trace) (data collected at APS-ANL) and comparison with other Ni(II) references including Ni(II) oxide (red trace), $Ni(OH)_2$ (green trace), $NiBO_3.xH_2O$ (purple trace), $NiFe_2O_4$ (olive trace).

Figure S7 shows the XANES spectrum of a sample of [NiSi]@NU-1000. The comparison of the energies of the pre-edge peaks of Ni and reference compounds is consistent with an oxidation state of +2 for Ni. Furthermore, comparison with Ni oxide indicates that the MOF material is not bulk NiO. No correspondence was found with Ni metal either (not shown here). Thus, this study is in agreement with a grafted Ni(II) species on the material.

While it was not possible to resolve the contributions of the expected Ni-O and Ni-P/Si scattering paths to generate a uniquely-good fit due to limited data in the EXAFS spectrum, qualitatively, the preliminary data are consistent with the proposed structure of the chemisorbed [NiSi]@NU-1000 material proposed in Scheme S1. This proposal is also based on other literature precedents. We propose that one [NiHSi(*o*-$C_6H_4CH_2PPh_2)_3$] fragment is bound to a $[Zr_6(\mu_3\text{-}O)_4(\mu_3\text{-}OH)_4(OH)_4(H_2O)_4]^{8+}$ cluster through the O atom of a hydroxyl ligand.[S2]

S2.2.5 SEM and SEM/EDX

Analyses by SEM (Scanning Electron Microscopy) and SEM/EDX (Energy Dispersive X-ray analysis) were performed on [NiSi]@NU-1000 (Figures S8 and S9). The results are in agreement with a homogenous distribution of Ni throughout the particles.

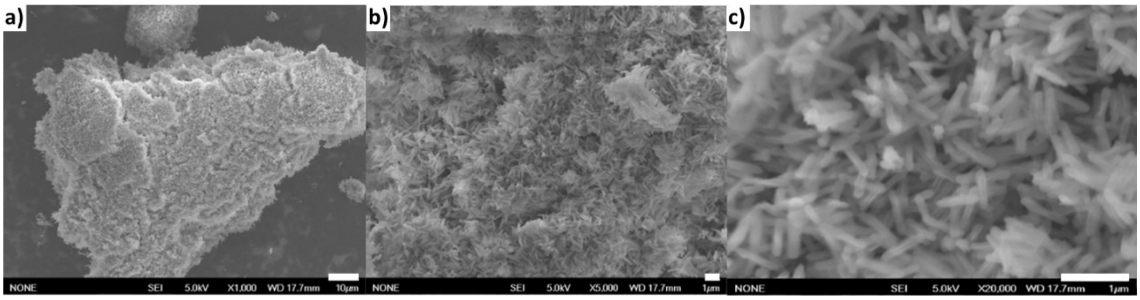

Figure S8. SEM images for [NiSi]@NU-1000 as synthesized. Scale bars indicate 10 μm for a), and 1 μm for b) and c).

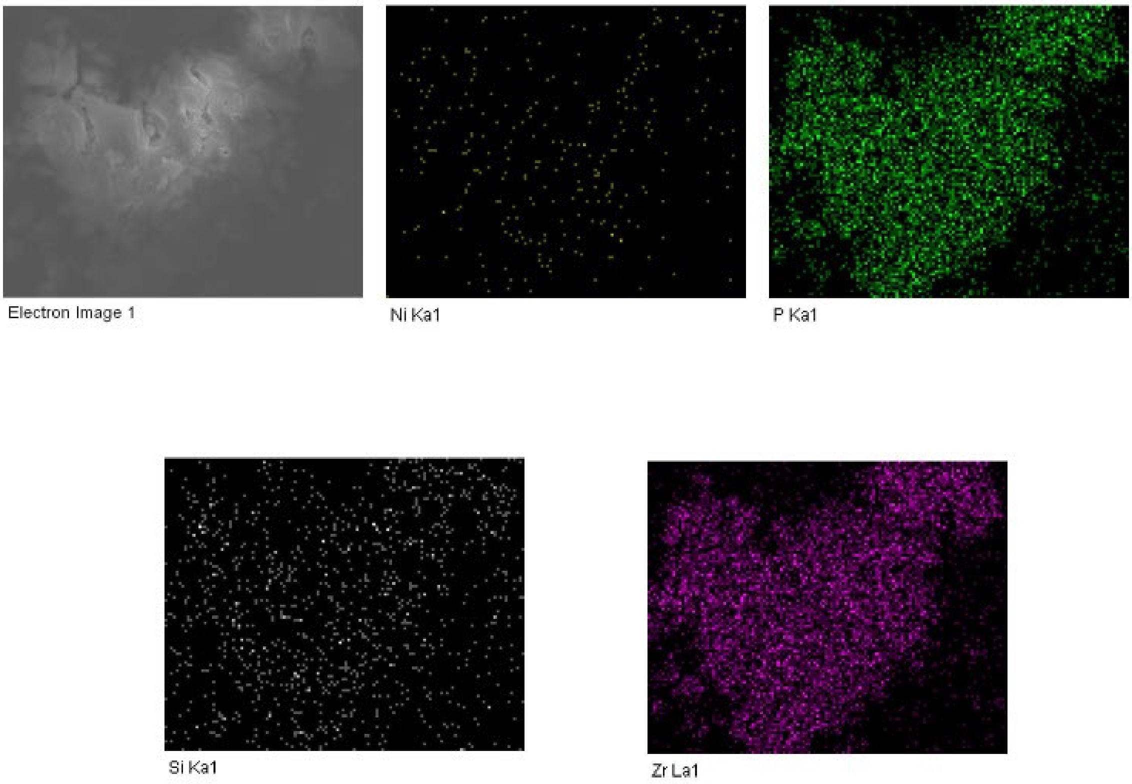

Figure S9. Electron images of material [NiSi]@NU-1000 confirming the presence of Ni, P, Si and Zr.

The SEM/EDX analyses confirm the presence of Ni, P, Si, and Zr in the sample, as shown in Figure S9. However, a quantitative determination of each element is not accurate as this is a surface technique, and the Ni organometallic complex is grafted onto the pores of the MOF material, as evidenced by the decrease in the BET surface area shown above in section S2.2.2. See also section 2.3.3, Table S3.

S2.2.6 TGA measurements

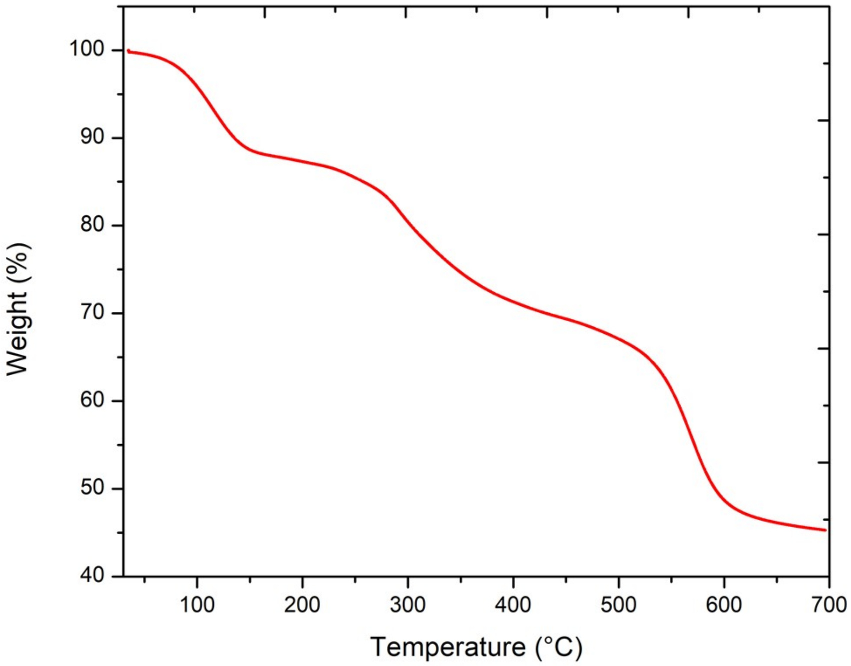

Figure S10. TGA analysis profile of [NiSi]@NU-1000.

S2.2.7 Solid-state UV-Vis spectroscopy

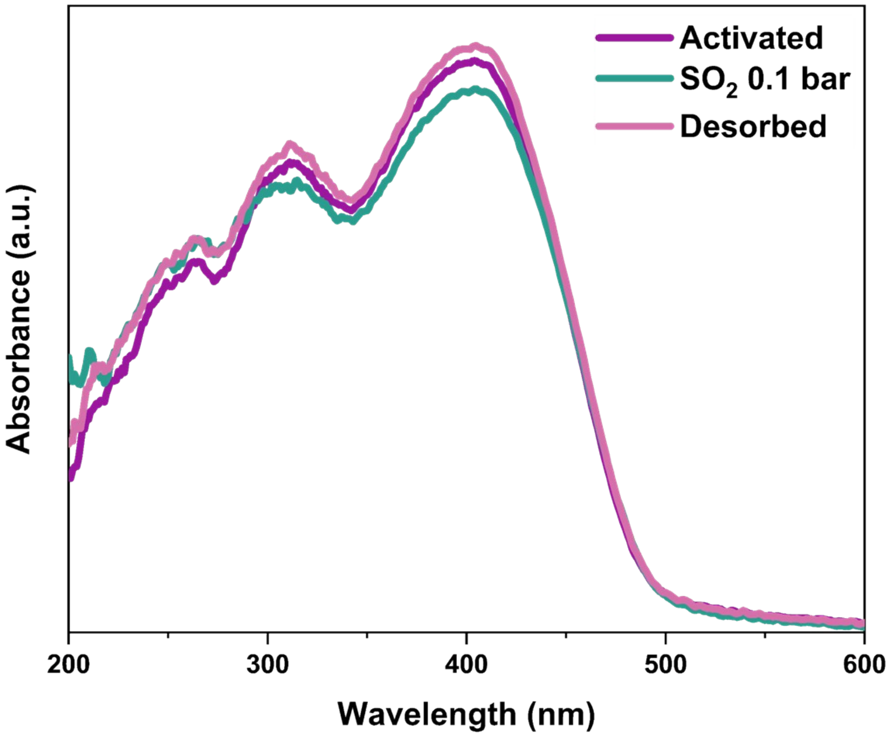

Figure S11. Solid-state UV-Vis diffuse reflectance spectra of [NiSi]@NU-1000: activated (purple line), after exposure to 0.1 bar of SO_2 (green line) and after desorption of SO_2 (pink line).

S2.2.8 IR Spectroscopy of the synthesized [NiSi]@NU-1000 material

ATR IR spectra of the [NiSi]@NU-1000 and the ungrafted NU-1000 were recorded and compared. The differences between the spectra of the NU-1000 and [NiSi]@NU-1000 materials are in accordance with the incorporation of the [NiSi] complex. The main differences encompass: (1) the appearance of a new band of medium intensity at 503.14 cm^{-1}, attributable to a Ni-O stretching vibration and, (2) changes in the number and intensity of the ν(Zr-O) vibrations in the region 644-730 cm^{-1} in agreement with the coordination of Ni to Zr-O(H) moieties (Figure S12).

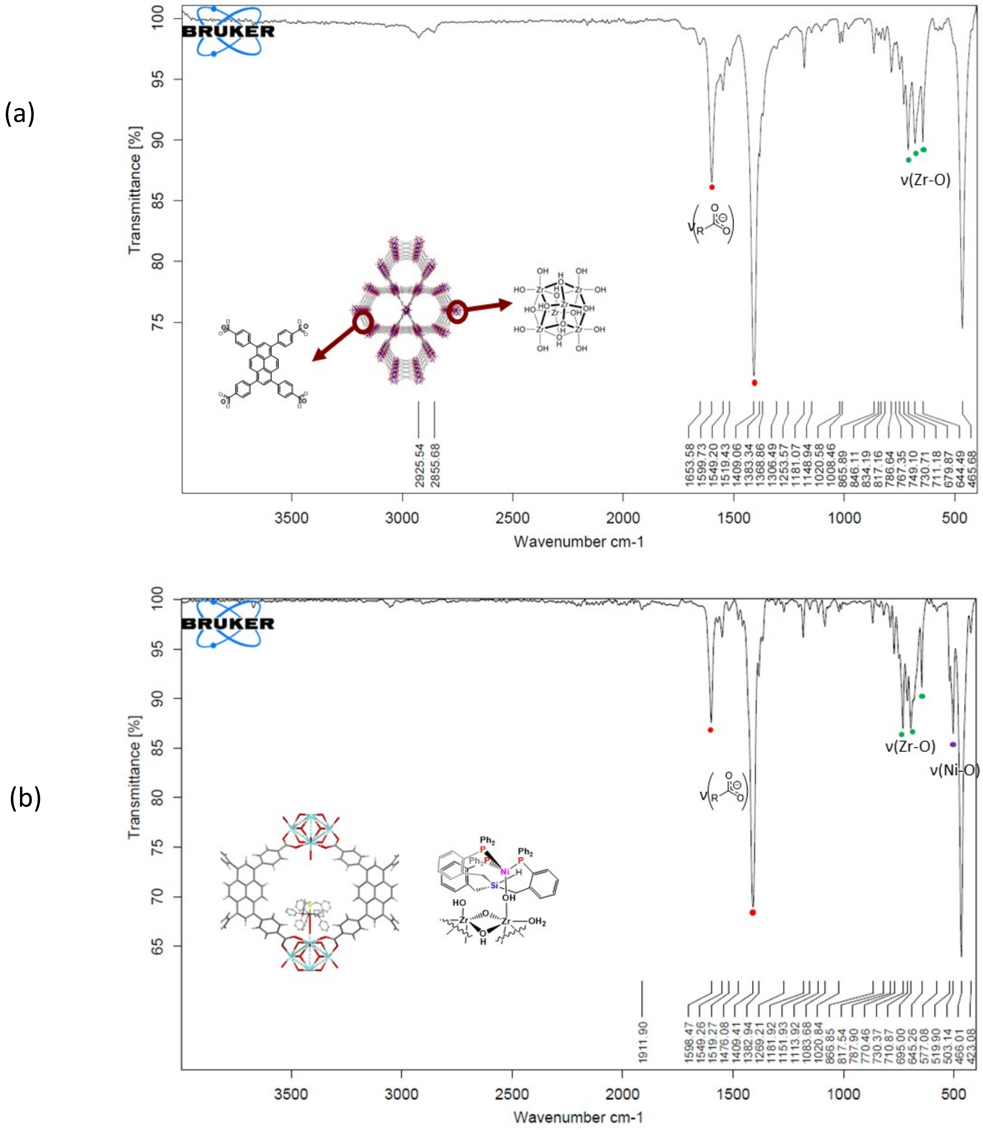

Figure S12. ATR-IR spectra of (a) unmodified NU-1000 and (b) grafted material [NiSi]@NU-1000.

S2.2.9 Nuclear Magnetic Resonance, ^{1}H NMR of digested samples

Nuclear magnetic resonance (NMR) experiments were performed on Bruker Avance III 300 MHz spectrometer operating with frequency, deuterated solvent (DMSO-d_6), and temperature indicated. The preparation of the samples for ^{1}H NMR followed the procedure reported in reference S1. The samples were digested using 5 drops of D_2SO_4 and sonicated to form a slurry. Then, 0.5 mL of DMSO-d_6 was added to dissolve the slurry and the solutions became clear. Under these conditions, we found only small differences between the spectra of the digested ungrafted NU-1000 material and the grafted [NiSi]@NU-1000 sample, in agreement with the 0.56 wt% of the Ni complex incorporated into the sample.[S2] Evidently, the changes are less discernible than in IR spectroscopy due to the lower sensitivity of NMR spectroscopy compared to IR. As anticipated, the presence of the pyrene linkers is ascertained. The small changes in the ^{1}H NMR spectrum of [NiSi]@NU-1000 involve the appearance of new broad features between 7.0-7.5 and at 2.7 ppm (highlighted in blue) which could be attributed to the aromatic hydrogens of the silylphosphine ligand in the organometallic [NiSi] complex which shows resonances at similar chemical shifts (**Figures S13** and **S1**). These new features are not present in the spectrum of the digested ungrafted NU-1000 material.

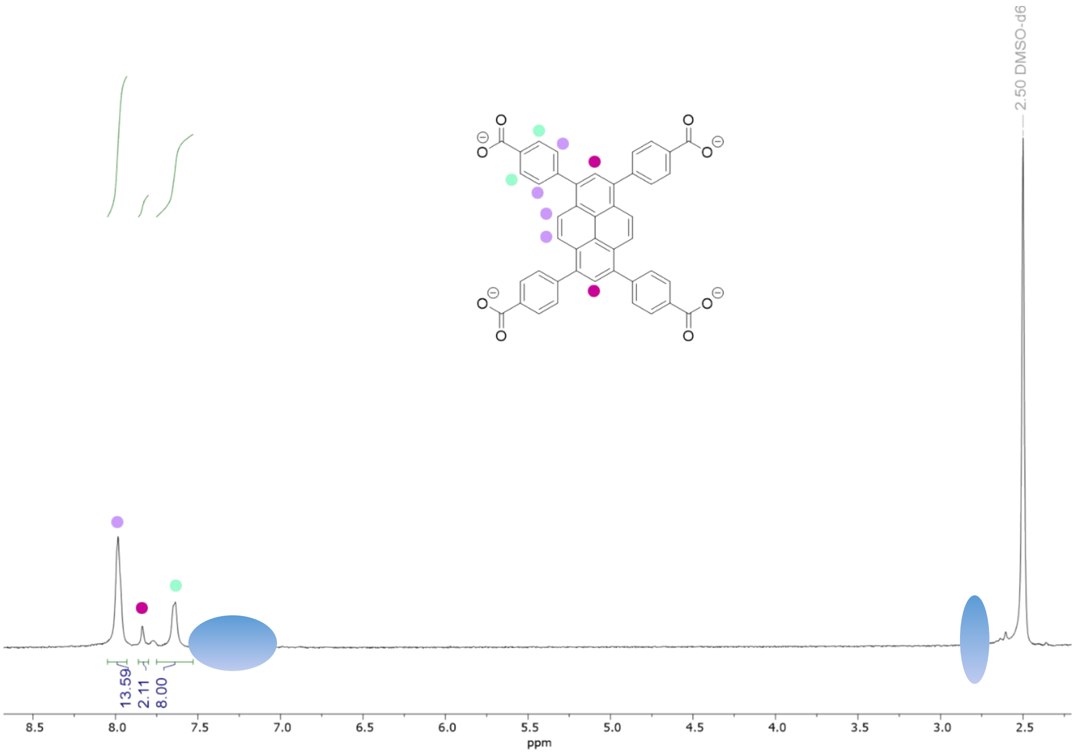

Figure S13. ^{1}H NMR spectrum (300 MHz, DMSO-d_6, 298 K) of digested [NiSi]@NU-1000. The spectrum closely resembles the one reported for digested NU-1000 except for small new features between 7.0-7.5 ppm and at 2.7 ppm which could be attributed to the aromatic hydrogens of the [NiSi] fragment.

S2.3 SO_2 adsorption experiments

S2.3.1 Adsorption-desorption isotherms of NU-1000 and [NiSi]@NU-1000

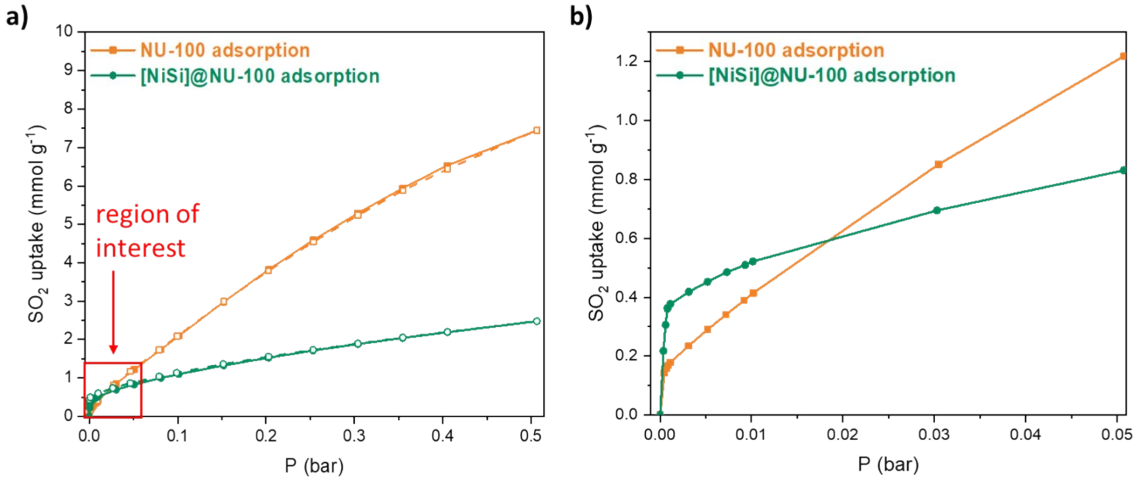

Figure S14. (a) Experimental SO_2 adsorption-desorption isotherm collected for a fully activated NU-1000 (orange) and [NiSi]@NU-1000 (green) sample (filled = adsorption; open = desorption) at 298 K and up to 0.5 bar; and (b) detail of adsorption at low pressures, below 0.05 bar.

Table S2. The adsorption capacities of SO_2 at low pressure on selected MOFs at 298 K.

Sample	**Surface area [m^2 g^{-1}]**	**SO_2 uptake [mmol g^{-1}]**				**-ΔH_{ads} of SO_2 [kJ mol^{-1}]**	**Ref.**
		0.002 bar	**0.005 bar**	**0.01 bar**	**0.05 bar**		
[NiSi]@NU-100	1354	0.404	0.453	0.515	0.831	42.7	This work
NU-1000	1970	0.202	0.290	0.415	1.219	50.8	[S3]
[Ir]@NU-100	1842	0.255	0.386	0.551	1.465	89.8	[S3]
[RuGa]@NU-100	1796	0.268	0.397	0.543	1.347	104.7	[S4]
SNFSIX-Cu-TPA	1169	2.22	2.95[a]	3.33	5.03[a]	58.81	[S5]
SIFSIX-Cu-TPA	1243	2.52	3.23[a]	3.80	5.41[a]	80.2	[S5]
Zr-Fum	600	~0.6[b]	~1.2[b]	1.2	~2.0[b]	49	[S6]
MOF-808	1990	~1.9[b]	~2.1[b]	2.1	~2.5[b]	n.a.	[S6]
DUT-67(Zr)	1260	~0.3[b]	~0.6[b]	0.7	~1.0[b]	n.a.	[S6]
Mg-gallate	576	4.65[c]	-	4.47[c]	-	60.3	[S7]
Co-gallate	494	3.99[c]	-	4.16[c]	-	55.6	[S7]
Ni-gallate	455	2.67[c]	-	3.37[c]	-	54.1	[S7]
Zr-bptc	960	-	~1.9[b]	~2.5[b]	~5.1[b]	45-50	[S8]
Zr-DMTDC	1345	-	~0.3[b]	~0.7[b]	~2.5[b]	32-29	[S8]
UiO-66	1221	-	~0.2[b]	~0.3[b]	~1.7[b]	37-27	[S8]
UiO-66-Cu^{II}	1068	-	~0.3[b]	~0.5[b]	~2.1[b]	38-34	[S8]
MFM-422	3296	-	-	~0.3[b]	~1.0[b]	26-19	[S8]
MFM-133	2156	-	-	~0.2[b]	~0.7[b]	31-27	[S8]
BUT-78	2031	0.77[a]	~1.1	1.33[a]	2.59[a]	39.0	[S9]

[a] Value estimated from the fitted isotherm data.

[b] Value estimated from the plotted isotherm.

[c] Value was originally reported in mmol cm^{-3} and transformed to mmol g^{-1} using the reported framework density.

S2.3.2 PXRD patterns before and after SO_2 experiments

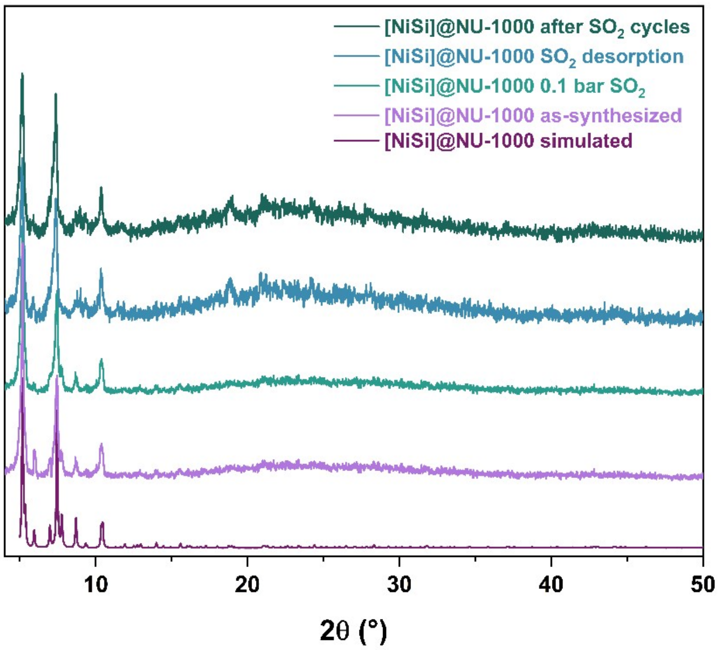

Figure S15. PXRD patterns of [NiSi]@NU-1000: as-synthetized after dry SO_2 adsorption and wet SO_2 exposure.

The PXRD measurements in Figure S15 corroborate the retention of the crystallinity and the material's stability after several SO_2 adsorption cycles. After each adsorption, the material was subjected to vacuum (1.7×10^{-3} Torr) for 45 minutes. The top two traces are obtained following five adsorption cycles of SO_2.

S2.3.3 EDX analysis before and after SO_2 exposure

Table S3. Ni(II) and associated sulphur occupancy were determined by measuring the Zr:Ni and Ni:S ratios using EDX analysis.

Sample	Ni occupancy (%)[a,b]	S occupancy (%)[a]	Std error (%)
([NiSi]@NU-1000) before SO_2 exposure	93		5.3
([NiSi]@NU-1000) after SO_2 exposure	90	2676.44	15.5

[a] Average atomic% obtained from three areas.

[b] Relative to full occupancy of Zr_6 atoms in the nodes of the NU-1000 framework

3

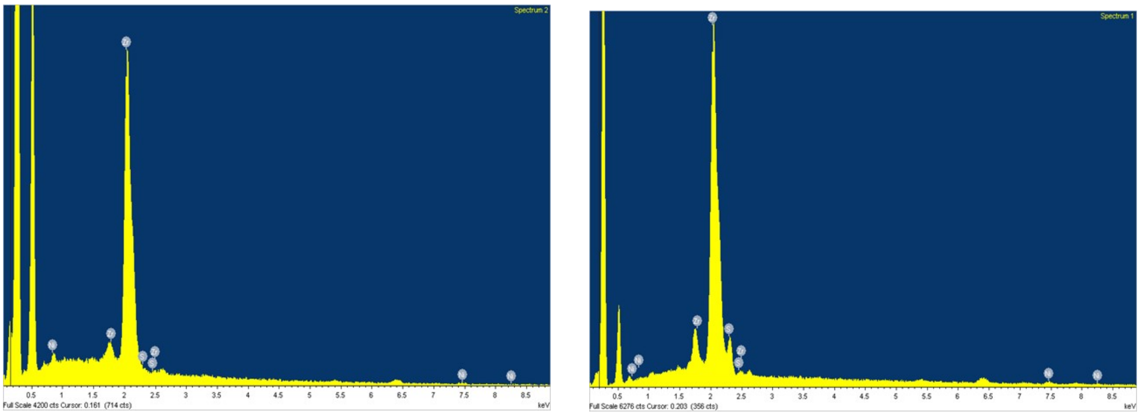

Figure S16. Representative raw EDX spectra for a) ([NiSi]@NU-1000) before SO_2 exposure; b) ([NiSi]@NU-1000) after SO_2 exposure.

These data show no evidence of changes in the amount of Ni before and after the SO_2 adsorption experiments. As expected, S is detected only after the adsorption experiments. One must, however, take into account that EDX is a surface technique, and the Ni organometallic complex is grafted onto the pores of the MOF material as previously disclosed. However, the similarity of the values of the Ni occupancy is meaningful and is in line with the preservation of the Ni complex.

S2.3.4 IR Spectroscopy before and after exposition to SO_2

The ATR-FTIR spectrum of the [NiSi]@NU-1000 material was also measured after the adsorption in the solid state of one atmosphere of SO_2 gas for one minute and compared with the corresponding spectrum before the adsorption. As evident in **Figure S17**, a colour change from pale to deep yellow is observed upon exposure of the sample to SO_2.

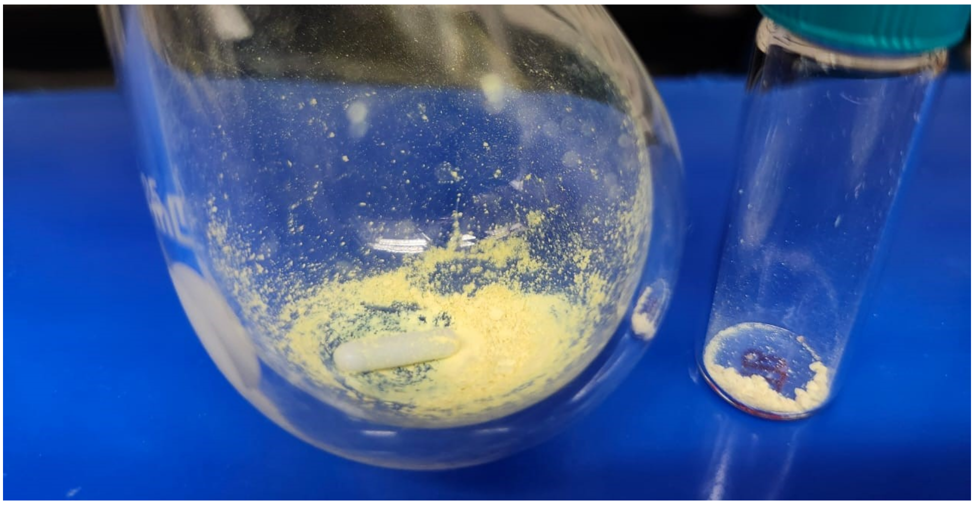

Figure S17. Photograph of the grafted material [NiSi]@NU-1000 before (right) and after exposure to 1 atmosphere of SO_2 (left).

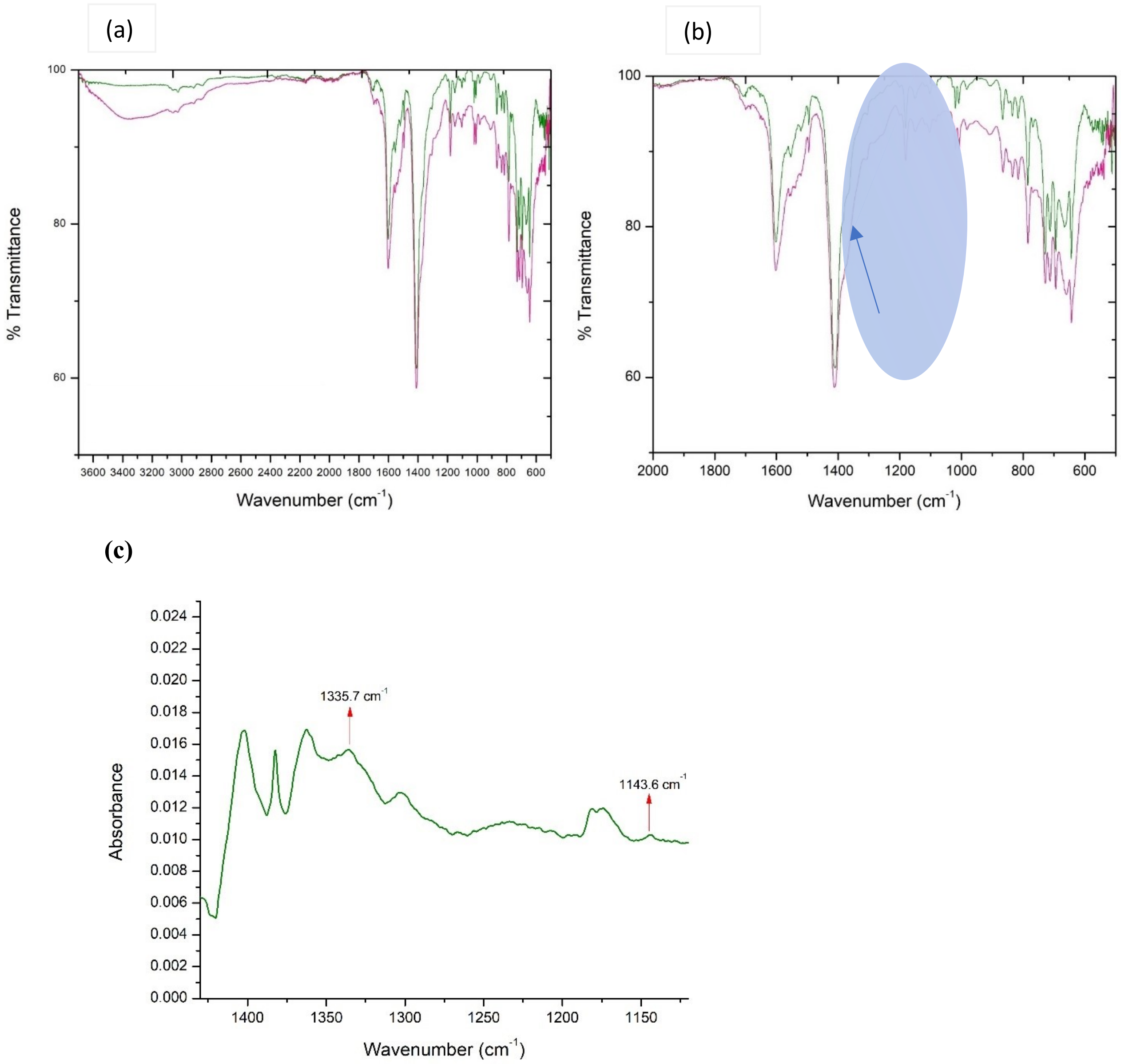

Figure S18. (a) ATR-FTIR spectrum of [NiSi]@NU-1000 before exposure (green) and after exposure to 1 atmosphere of SO_2 (pink). (b) Expanded region of the ATR-FTIR spectrum where major changes are highlighted in blue. (c) Expanded region of a difference spectrum (plotted in Absorbance). The subtraction shown was a factor of 1.06 of the material before exposure from the spectrum after adsorption of one atmosphere of SO_2. The positive features at 1336 and 1144 cm^{-1} correspond to the physisorption of the gas.

In **Figure S18**, the ATR-FTIR spectra before and after absorption are shown. Although the region of interest (1400-1100 cm^{-1}) is partially obscured by the infrared absorptions of the material, we consistently observe growing features at 1336 cm^{-1} (broad) and 1144 cm^{-1} (vw) in the difference IR spectrum. These features could be assigned respectively to the ν_3 asymmetric and ν_1 symmetric bands of the adsorbed SO_2 and are thus consistent with physisorption of SO_2. Similarly, in the Ni(II) based material BUT-78, adsorption of SO_2 results in $\nu(SO_2)$ vibrations at 1140 and 1330 cm^{-1} [S9] whereas Cu based MFM-170 shows the ν_1 adsorption at 1143 cm^{-1} and the ν_3 between 1320 and 1340 cm^{-1} depending on the SO_2 pressure.[S10] Thus, small redshifts for the vibrational modes are observed in comparison to free SO_2 gas at 1151(w) and 1362(s) cm^{-1} [S11] or 1147 (w) and 1357(s) cm^{-1}.[S12]

S2.3.5 Isosteric enthalpy of SO_2 adsorption

The enthalpy of adsorption of SO_2 for [NiSi]@NU-1000 was calculated according to the virial method reported in the literature.[S3] Briefly, two experimental adsorption isotherms (298 and 308 K) were fitted using the following virial equation:

$$\ln p = \ln n + \frac{1}{T}\sum_{i=0}^{m} a_i n^i + \sum_{j=0}^{k} b_j n^j \qquad \text{Eq. S1}$$

where p is the pressure (kPa), n is the adsorbed amount (mml g^{-1}), T is the temperature (K), and a_i or b_j are the virial coefficients. The isotherms data was plotted as $ln\text{p}=f(\text{n})$ to carry out the fitting (Figure S19a). The enthalpy of adsorption as a function of the surface coverage (Figure S19b) was calculated, from the virial fitted parameters using the following equation:

$$\Delta H_{ads} = R\sum_{i=0}^{m} a_i n^i \qquad \text{Eq. S2}$$

where R is the universal gas constant (8.314 J mol^{-1} K^{-1}). The ΔH_{ads} near zero coverage was estimated using only the a_0 virial coefficient in eq. S2, obtaining -42.7 kJ mol^{-1}.

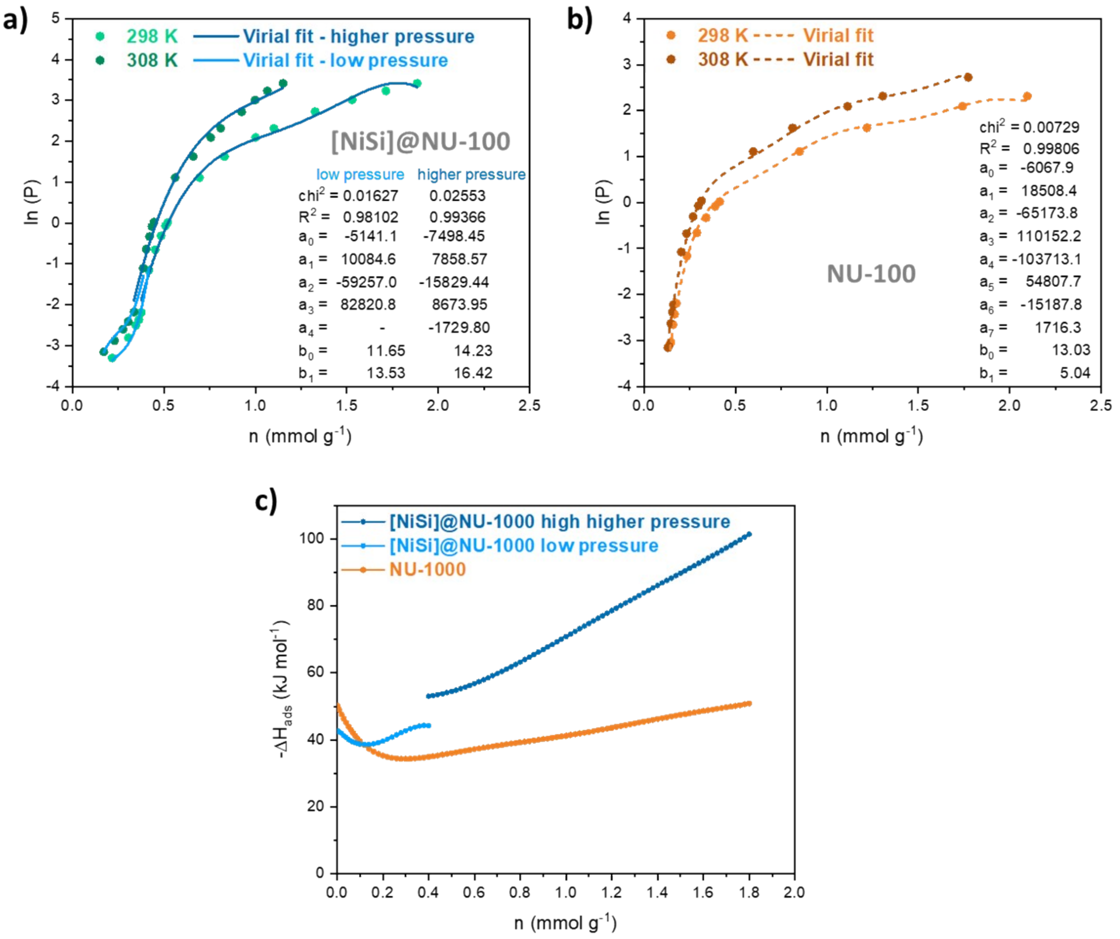

Figure S19. Virial fittings for SO_2 adsorption isotherms at 298 and 308 K, a) for the [NiSi]@NU-1000 material, separated in two sections: low pressure (light blue) and higher pressure (navy blue), and b) for the NU-1000. c) Isosteric enthalpy of adsorption of SO_2 for [NiSi]@NU-1000 and NU-1000.

S2.3.6 System for *in situ* wet SO_2 exposure experiments

The system (Figure S20) contains two principal parts:

A. The gas generator, in which Na_2SO_3 is added to a two-neck ball flask [1], which is capped with a rubber stopper through which Na_2SO_3 is injected with a syringe [2]. One is covered with a rubber stopper through which concentrated H_2SO_4 is injected with a glass syringe [2], while the other is covered with a rubber stopper [3]. Concentrated H_2SO_4 [2] is injected through a glass syringe, while the other port is connected to the saturation chamber.

B. The saturation chamber, made of a round flask [3], is connected to a vacuum line [4] and a vacuum line [4]. Vacuum line [4] and a pressure gauge [5].

To start the process, a sample of about 20 mg in a 1.5 mL glass vial was activated in a sand bath at 423 K under vacuum for 24 h. The sample was then placed in the saturation chamber, and the system was evacuated with a vacuum line. The vial was then placed in the saturation chamber, and the system was evacuated with a vacuum line. Next, 1 bar of SO_2 gas was generated by dripping 1.2 mL of concentrated H_2SO_4 over 2 g of Na_2SO_3; the sample was left continuously exposed to the gas for 3 hours. For the sample exposed to 0.1 bar SO_2, the sample was activated in the same way, and 0.12 mL of concentrated H_2SO_4 was dripped onto 0.2 g of Na_2SO_3. The sample was left continuously exposed to the gas for 3 hours.

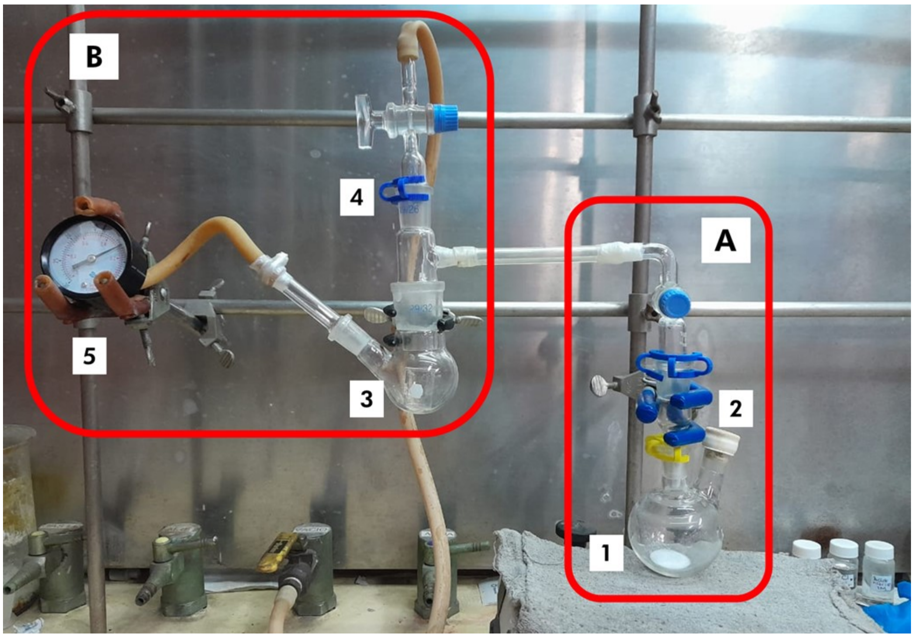

Figure S20. Homemade system for wet SO_2 adsorption experiments.

S2.3.7 Fluorescence and time-resolved photoluminescence TRPL experiments before and after SO_2 exposure

S2.3.7.1 Fluorescence experiments of the pristine material

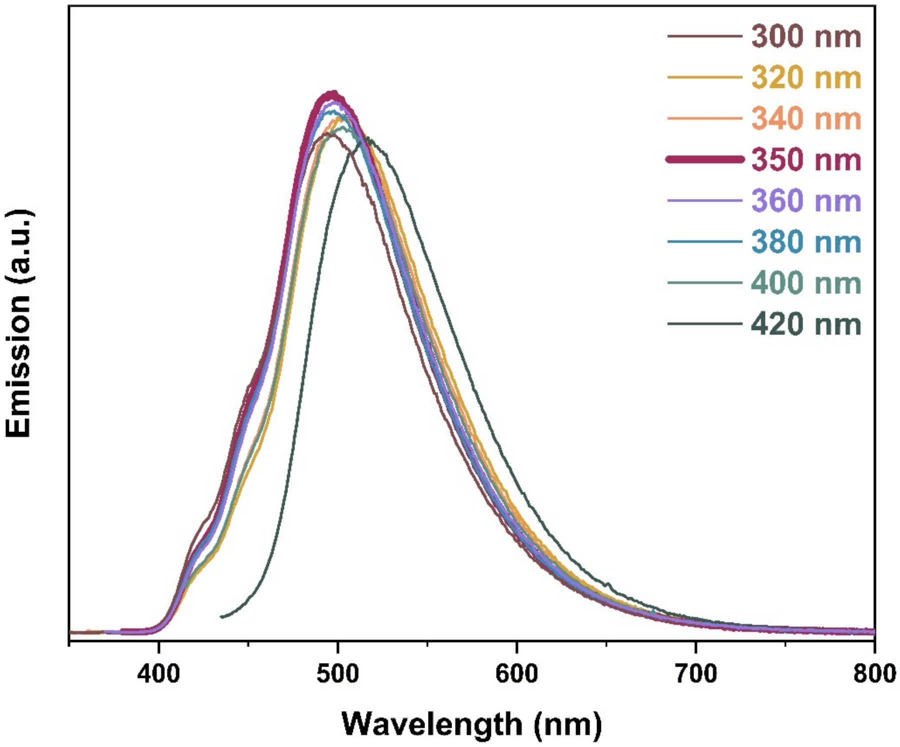

Figure S21. Solid-state emission spectra of activated [NiSi]@NU-1000 at the different excitation wavelengths.

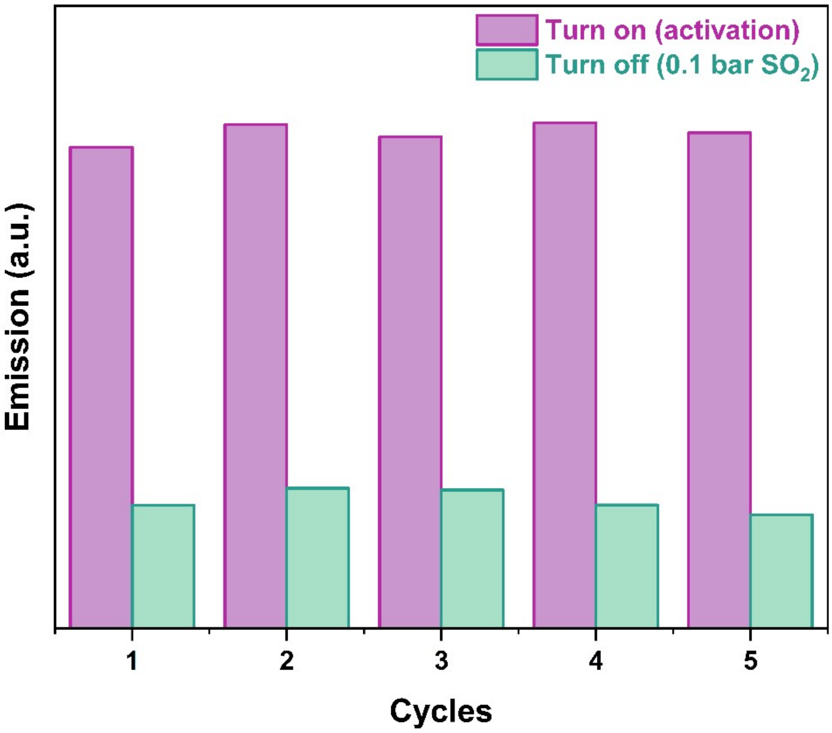

Figure S22. Cycling of five emission intensities for activated [NiSi]@NU-1000 and SO_2-saturated [NiSi]@NU-1000 measured at 350 nm excitation.

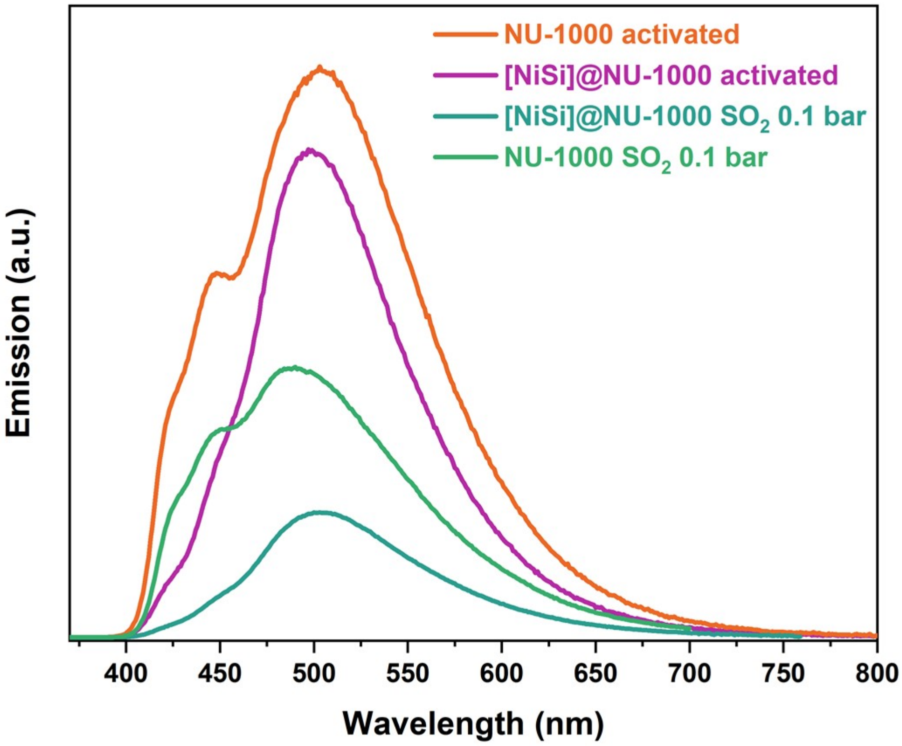

Figure S23. Solid-state emission spectra of activated NU-1000 and [NiSi]@NU-1000 before and after SO_2.

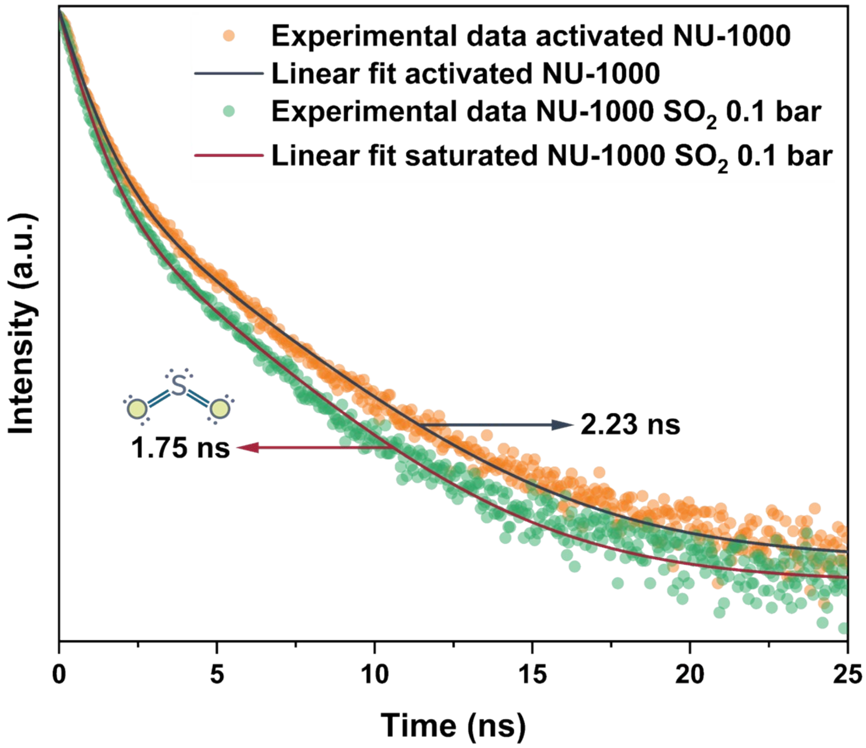

Figure S24. Time-resolved photoluminescence decay spectra of activated NU-1000, and after exposure to 0.1 bar of SO_2 measured at 335.6 nm excitation and at 500 nm emission.

Fluorescence lifetimes were determined from the TPRL spectra. The data obtained from the decay spectra were fitted in Fluoracle software, using a multi-exponential equation to describe the fluorescence emission decay curve:

$$R(t) = B_1 e^{\left(\frac{-t}{\tau_1}\right)} + B_2 e^{\left(\frac{-t}{\tau_2}\right)} + B_3 e^{\left(\frac{t}{\tau_3}\right)} \qquad \text{Eq. S3}$$

where R(t) represents the fluorescence intensity as a function of time, B_1, B_2 and B_3 are the amplitudes of the respective decay components, and τ_1, τ_2 and τ_3 are the lifetimes of the different components.

Table S3 shows the τ_n values and their corresponding contributions to the fluorescence lifetime of each measurement. Additionally, the χ^2 value is reported, which, in this type of analysis, represents the quality of the fit of the model to the experimental data.

Table S4. Average decay lifetime and lifetime components fitted from the TRPL decay spectra of activated and SO_2 saturated [NiSi]@NU-1000 samples.

	Activated [NiSi]@NU-1000	**SO_2-saturated [NiSi]@NU-1000**	**Activated NU-1000**	**SO_2-saturated NU-1000**
τ_1 (ns)	0.0540	0.0715	0.1899	0.1045
a_1	0.2410	0.3167	0.2665	0.3006
τ_2 (ns)	1.3895	1.1675	1.4330	1.1956
a_2	0.5508	0.5084	0.4643	0.4600
τ_3 (ns)	5.4151	4.3245	5.6135	4.8625
a_3	0.2082	0.1749	0.2692	0.2395
Fluorescence lifetime (ns)	**1.9068**	**1.3726**	**2.2271**	**1.7475**
χ^2	1.57	1.33	1.40	1.41

S2.3.8 Possible modes of SO_2 interaction within [NiSi]@NU-1000

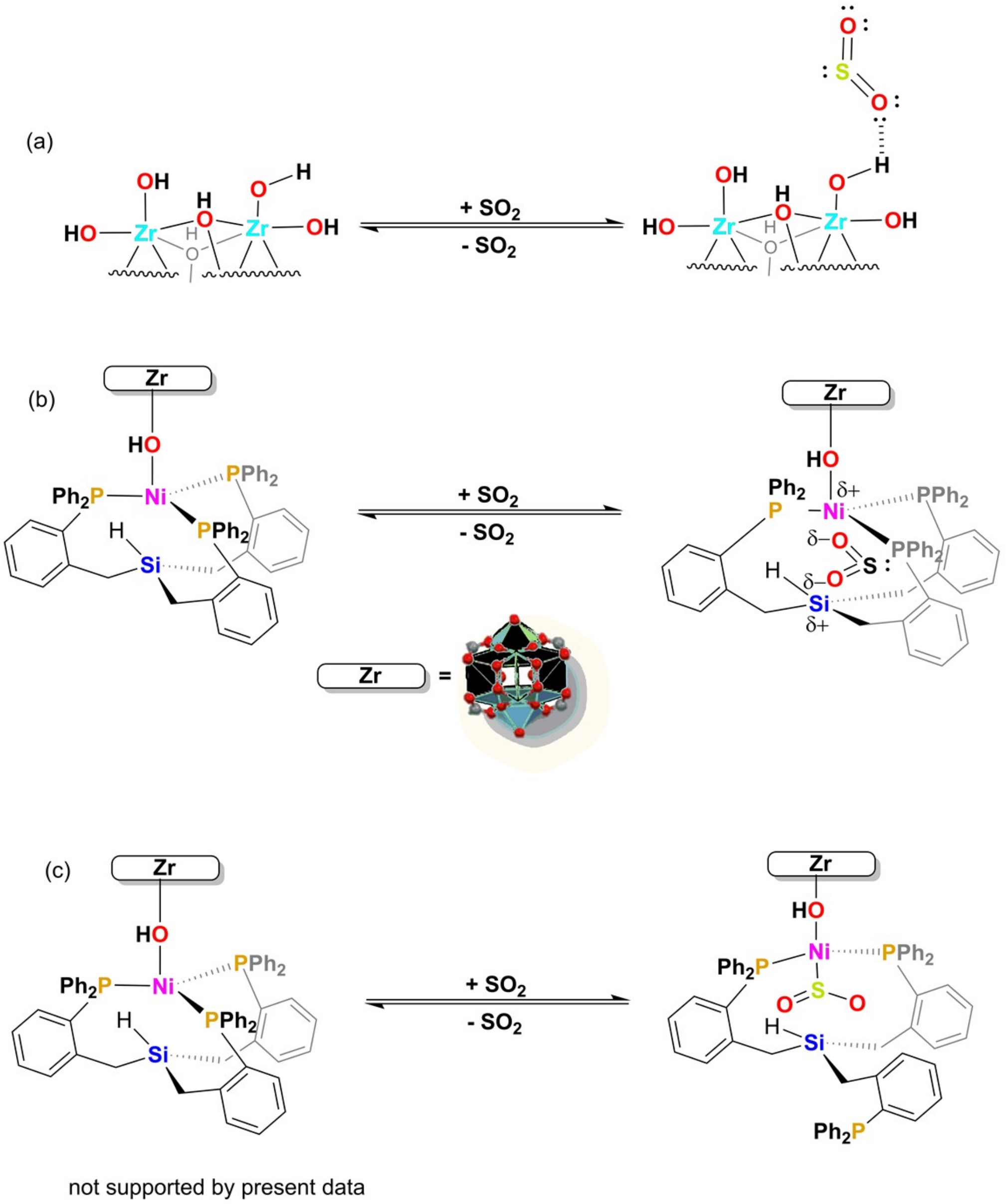

Figure S25. Proposed adsorption mechanisms for SO_2 on the [NiSi]@NU-1000 material. (a) The hydroxyl groups over the $[Zr_6(\mu_3\text{-}OH)_8(OH)_8]$ node serve as hydrogen-bond donors for the SO_2 molecules; this has been reported as primary adsorption sites for other Zr-based MOFs: UiO-66, Zr-bptc and MFM-601.[S8,S14] (b) Electrostatic interactions of SO_2 molecules with the Ni and Si centers could be established explaining the enhancement on the grafted material's response. A chemisorption process involving the formation of a Ni-SO_2 bond is not sustained by the present results, although this type of coordination has been observed in other molecular systems.[S16, S17]

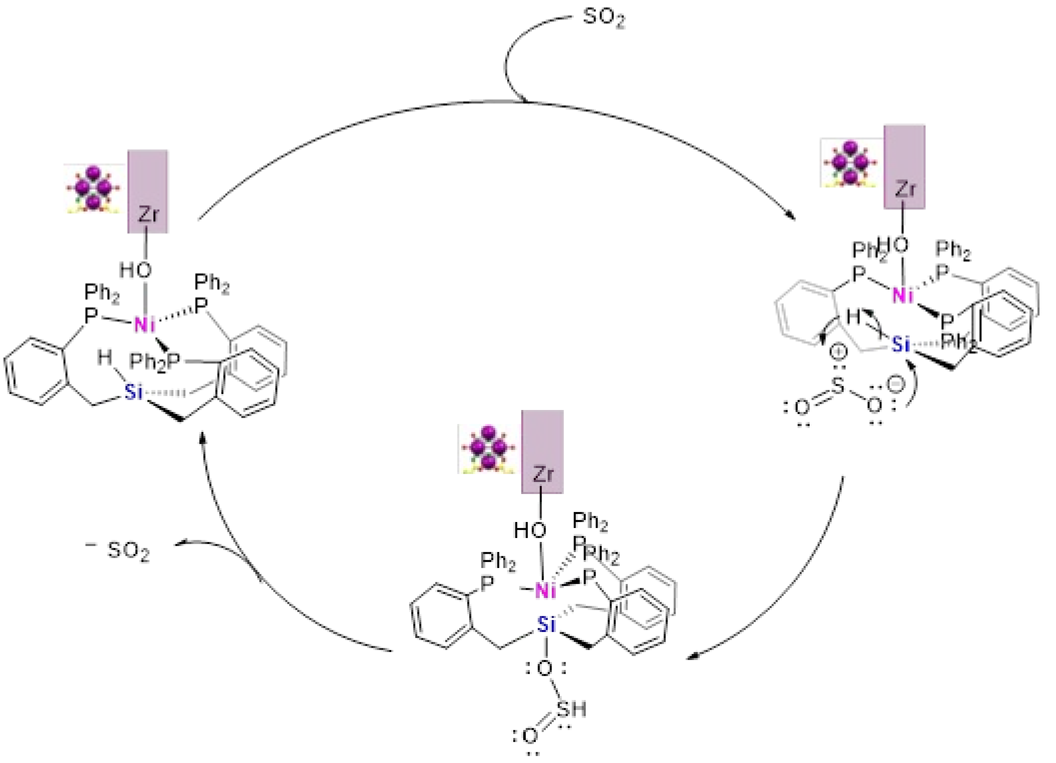

Figure S26. An alternative less-conventional computed mechanism for the reactivity of the [NiSi]@NU-1000 material and SO_2. Given that a dangling Si-H fragment could potentially be the catalytic center, as has been demonstrated in reference S2 with carbonylic substrates, another possibility is given, which involves a four-member metathesis-like intermediate, as shown.

An alternative, though less conventional, mechanism is shown in Figure S26. The interaction of an SO_2 molecule with the [NiSi] complex grafted to the NU-1000 was probed by a computational model. This model only contains the most relevant atoms from the [NiSi] complex. The SO_2 molecule was allowed to interact with five different positions of the organometallic fragment (Figure S27). Full geometry optimisations were performed with Gaussian 09 code at B3LYP/6-31+g (2d, p) level of theory.[S15] Partial optimisations indicated the migration of one hydrogen atom from the Si complex to the S atom of the SO_2 molecule. The most stable structure was calculated at 231.2 kcal mol^{-1}, which was demonstrated to be more stable than the initial geometry and exhibited the hydrogen atom bonded to the S atom from the SO_2 molecule. It is worth emphasising that different initial geometries result in the same final optimised structure.

Although these results give some indication of the plausibility of the mechanistic pathway in Figure S26, given the values obtained for the isosteric enthalpy of adsorption and the information gathered also from IR spectroscopy in agreement with a physisorption process, we favor the proposed mechanism in Figures S25 a and b.

Partial SO_2 optimization

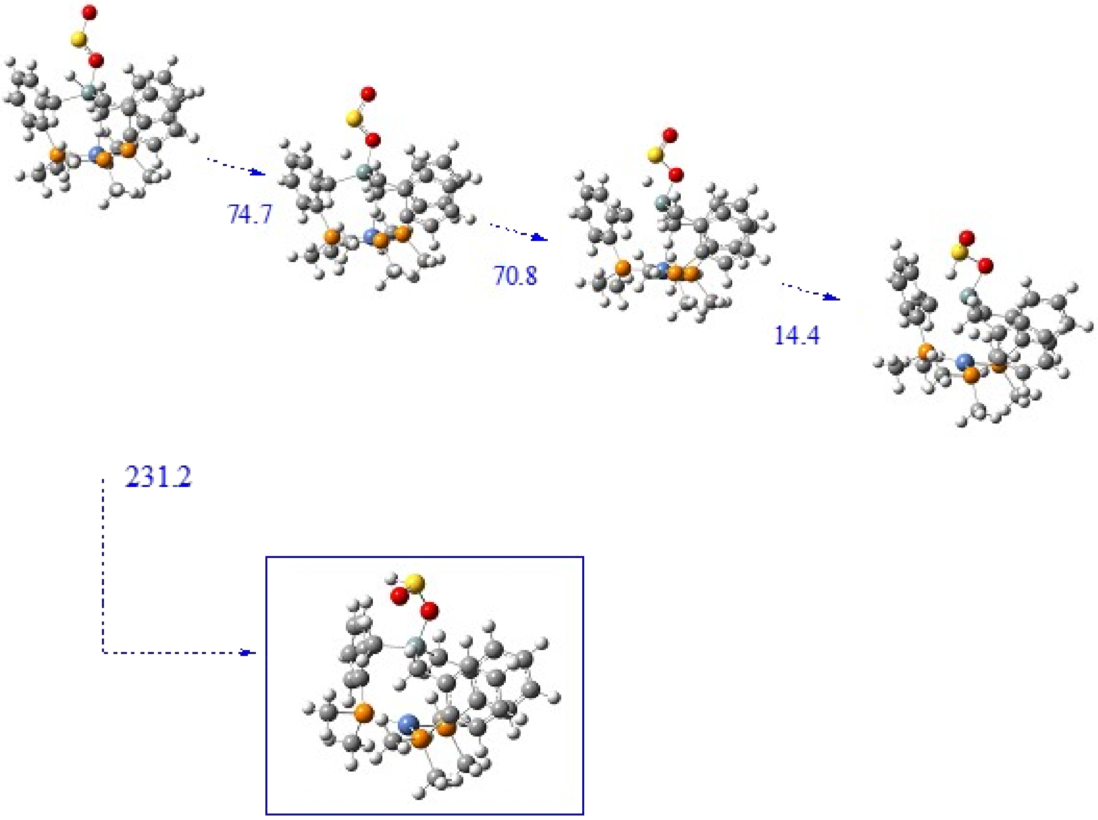

Figure S27. Partial optimisations and the most stable structure (inside the blue square) for the proposed mechanism in Figure S25. Values are energy differences in kcal mol^{-1}.

S3. References

[S1] T. C. Wang, N. A. Vermeulen, I. S. Kim, A. B. F. Martinson, J. F. Stoddart, J. T. Hupp and O. K. Farha, *Nat. Protoc.,* 2016, **11**, 149–162.

[S2] L. J. Barrios-Vargas, N. S. Abeynayake, C. Secrist, N. Le, C. E. Webster, B. Donnadieu, D. M. Kaphan, A. D. Roy, I. A. Ibarra and V. Montiel-Palma, *Dalton Trans.,* 2023, **52**, 8883–8892.

[S3] S. Gorla, M. L. Díaz-Ramírez, N. S. Abeynayake, D. M. Kaphan, D. R. Williams, V. Martis, H. A. Lara-García, B. Donnadieu, N. Lopez, I. A. Ibarra and V. Montiel-Palma, *ACS Appl. Mater. Interfaces,* 2020, **12**, 41758–41764.

[S4] J. García Ponce, M. L. Díaz-Ramírez, S. Gorla, C. Navarathna, G. Sanchez-Lecuona, B. Donnadieu, I. A. Ibarra and V. Montiel-Palma, *CrystEngComm,* 2021, **23**, 7479–7484.

[S5] W. Li, C. Cheng, G. Gao, H. Xu, W. Huang, Z. Qu and N. Yan, *Mater. Horiz.*, 2024, **11**, 1889–1898.

[S6] P. Brandt, S. H. Xing, L. Liang, G. Kurt, A. Nuhnen, O. Weingart and C. Janiak, *ACS Appl. Mater. Interfaces,* 2021, **13**, 29137–29149.

[S7] F. Chen, D. Lai, L. Guo, J. Wang, P. Zhang, K. Wu, Z. Zhang, Q. Yang, Y. Yang, B. Chen, Q. Ren and Z. Bao, *J. Am. Chem. Soc.,* 2021, **143**, 9040–9047.

[S8] J. Li, G. L. Smith, Y. Chen, Y. Ma, M. Kippax-Jones, M. Fan, W. Lu, M. D. Frogley, G. Cinque, S. J. Day, S. P. Thompson, Y. Cheng, L. L. Daemen, A. J. Ramirez-Cuesta, M. Schröder and S. Yang, *Angew. Chem. Int. Ed.,* 2022, **61**, e2022072.

[S9] Si, G. R.; Kong, X. J., He, T.; Zhang, Z.; Li, J. R. *Nat. Commun.,* 2024, **15**, 7220

[S10] G. L. Smith, J. E. Eyley, X. Han, X. Zhang, J. Li, N. M. Jacques, et al., *Nat. Mater.* 2019, **18**, 1358–1365.

[S11] A. L. Goodman, P. Li, C. R. Usher and V. H. Grassian, *J. Phys. Chem. A* 2001, **105**, 6109-6120

[S12] A. K. Brisdon, *Inorganic Spectroscopic Methods*, Oxford University Press, 1998.

[S13] A. Nuhnen and C. Janiak, *Dalton Trans.*, 2020, **49**, 10295–10307.

[S14] J. H. Carter, X. Han, F. Y. Moreau, I. da Silva, A. Nevin, H. G. W. Godfrey, C. C. Tang, S. Yang and M. Schröder, *J. Am. Chem. Soc.*, 2018, **140**, 15564–15567.

[S15] M.J. Frisch, G.W. Trucks, H.B. Schlegel, G.E. Scuseria, M.A. Robb, J.R. Cheeseman, J.J.A. Montgomery, T. Vreven, K.N. Kudin, J.C. Burant, J.M. Millam, S.S. Iyengar, J. Tomasi, V. Barone, B. Mennucci, M. Cossi, G. Scalmani, N. Rega, G.A. Petersson, H. Nakatsuji, M. Hada, M. Ehara, K. Toyota, R. Fukuda, J. Hasegawa, M. Ishida, T. Nakajima, Y. Honda, O. Kitao, H. Nakai, M. Klene, X. Li, J.E. Knox, H.P. Hratchian, J.B. Cross, V. Bakken, C. Adamo, J. Jaramillo, R. Gomperts, R.E. Stratmann, O. Yazyev, A.J. Austin, R. Cammi, C. Pomelli, J.W. Ochterski, P.Y. Ayala, K. Morokuma, G.A. Voth, P. Salvador, J.J. Dannenberg, V.G. Zakrzewski, S. Dapprich, A.D. Daniels, M.C. Strain, O. Farkas, D.K. Malick, A.D. Rabuck, K. Raghavachari, J.B.

Foresman, J.V. Ortiz, Q. Cui, A.G. Baboul, S. Clifford, J. Cioslowski, B.B. Stefanov, G. Liu, A. Liashenko, P. Piskorz, I. Komaromi, R.L. Martin, D.J. Fox, T. Keith, M.A. Al-Laham, C.Y. Peng, A. Nanayakkara, M. Challacombe, P.M.W. Gill, B. Johnson, W. Chen, M.W. Wong, C. Gonzalez and J.A. Pople. GAUSSIAN 09 (Revision A.08), Inc. Wallingford, CT, 2009.

[S16] W. A. Schenk, *Dalton Trans.*, 2011, **40**, 1209.

[S17] A. V. Marchenko, A. N. Vedernikov, J. C. Huffman and K. G. Caulton. *New J. Chem.,* 2003, **27**, 630.